ELSEVIER

Three-component layer double hydroxides by urea precipitation: structural stability and electrochemistry

Bora Mavis, Mufit Akinc*

Ames Laboratory and Materials Science and Engineering Department, 3053 Gilman Hall, Iowa State University, Ames, IA 50011, USA

Abstract

Three-component layer double hydroxides (LDHs) with varying compositions were produced by urea precipitation, and tested for their stability and electrochemical performance. Optimum initial metal ion concentrations in the starting solutions were established. Initial Al^{3+} concentration in the solution needs to be at least 0.015 M for the LDH formation. From the solutions with initial Al^{3+} concentration of 0.025 M, higher fractions of Ni^{2+} and Co^{2+} could be recovered. Co^{2+} could be incorporated at various levels without disturbing the LDH structure. LDH structure proved stable once it formed. Cyanate in the LDHs was dominantly N-bonded which contributed to the stability of the structure. Highest specific discharge capacity delivered by a LDH was 336 mAh/g, which was about 30% higher than that by β-Ni(OH)$_2$. LDHs reached their stable capacities at a lower rate than either β-Ni(OH)$_2$ or the interstratified-Ni(OH)$_2$ (α + β). The interstratified sample delivered the highest capacity compared to any of the tested compositions.
© 2004 Elsevier B.V. All rights reserved.

Keywords: Nickel hydroxide; Layer double hydroxides; Urea precipitation; FTIR; Electrochemistry

1. Introduction

Nickel hydroxide is used in the positive electrode of the rechargeable alkaline batteries based on nickel, e.g. Ni/Cd, Ni/Zn, Ni/MH. It has two polymorphs, namely β and α, both of which consists of brucite-type layers. Two polymorphs are different in the stacking of these layers. Layers can be well-ordered and closely packed along the *c*-axis as in the β-phase (interlayer separation ≈4.6 Å) or could be randomly stacked along the *c*-axis with water or anionic intercalates residing within the Van der Waals gap as in the α-phase. Intercalating species result in a larger interlayer separation (7–8 Å depending on the size and bonding of the intercalating species) [1–4]. α-Phase transforms to β-phase upon exposure to the common electrolyte (6 M KOH) used in this battery system.

In general, it is assumed that there is a hydroxyl deficiency in the basal planes of α-phase that would permit the intercalation of negatively charged anions within the interlayer spacing. This could be represented with the formula Ni(OH)$_{2-x}$(A^{n-})$_{x/n}$·mH$_2$O, where A represents the anion. Hydroxyl deficiency can be compensated by the direct in-sertion of the anion for the hydroxide site. Another alternative mode of intercalation is the intercalation of the free anion between the basal planes. For this alternative to be realized, it is assumed that all hydroxyls are in their crystallographically defined sites and a positively charged layer (i.e. protonated layer, [Ni(OH)$_{2-x}$(H$_2$O)$_x$]$^{x+}$) exists [1,5,6]. Yet another possibility is the existence of a trivalent cation within the basal planes which would permit both modes of anion intercalation [6].

Intercalation compounds that are represented by [M$_{1-x}$$^{2+}$ M$_x$$^{3+}(OH)_2$]$^{x+}$[A$_{x/n}$$^{n-}$]$^{x-}$ · mH$_2$O has been investigated under the name layer double hydroxides (LDHs). These compounds have also been referred to as hydrotalcite-like compounds, mixed metal-layered hydroxides or anionic clays. Again stacking of brucite-like octahedral layers forms their crystal structure. Direct substitution of the divalent cation (M^{2+} can be Mg^{2+}, Mn^{2+}, Fe^{2+}, Co^{2+}, Ni^{2+}, Cu^{2+}, Zn^{2+}, or Ca^{2+}, etc.) with a trivalent ion (M^{3+} can be Al^{3+}, Cr^{3+}, Mn^{3+}, Fe^{3+}, Co^{3+}, Ni^{3+}, etc.) creates a permanent positive layer charge. This necessitates the intercalation (A^{n-} can be selected from a wide range of inorganic anions, organic anions and complexes) between the layers as charge balancing species [7–9].

Co^{2+} is known to irreversibly oxidize to Co^{3+} during charging and claimed to supply such an extra charge to the

* Corresponding author. Tel.: +1-515-294-0738; fax: +1-515-294-5444.
E-mail address: makinc@iastate.edu (M. Akinc).

layers when used in the $Ni(OH)_2$ system [10,11]. It is possible to use urea precipitation method in order to produce pure α-$Ni(OH)_2$'s [2,12–18] or cobalt doped α-$Ni(OH)_2$'s that are more or less stable under electrochemical cycling [19].

Use of a trivalent cation like Al^{3+} (i.e. producing a Ni/Al LDH) has proven to be another effective method of increasing the stability of α-phase in the electrolyte [20,21]. Costantino et al. reported the first use of urea precipitation method in producing Ni/Al LDHs. Nevertheless their main focus was to prepare intercalation compounds with alkoxides and they did not study their electrochemical properties [22].

Concurrent to this work, a number of articles have appeared on the electrochemical properties of the Ni/Al-based LDHs [23–27]. Maximum reported capacities were 238 mAh/g at 1C rate [27], 303 mAh/g at 0.33C rate [26] and 340 mAh/g at 0.2C rate. In two most recent studies three-component LDHs (TC-LDHs) were produced and tested: Ni/Al/Zn resulted in 425 mAh/g at C rate [28] and Ni/Al/Co which could be obtained only as a turbostratic phase delivered 319 mAh/g at about 0.2C rate [29]. Wang et al. have recently reported an interesting result from a "nanostructural multiphase" $Ni(OH)_2$ (i.e. interstratified α- and β-phases) produced by doping $Ni(OH)_2$ with various levels of Co, Zn, and Mn [4]. At least in one case they were able to obtain a capacity of 375 mAh/g at 0.2C.

To our knowledge precipitation of a TC-LDH with urea decomposition has not been reported. Furthermore, in the sole attempt with Ni/Al/Co, the LDH structure was not observed [29]. We explored the viability of urea precipitation as a method to produce Ni/Al/Co TC-LDHs and tested their stability and electrochemical characteristics, and compared with a commercially available β-$Ni(OH)_2$ sample and a sample with interstratified structure which was produced by heterogeneous precipitation.

2. Experimental method

2.1. Powder synthesis and aging

Precipitation of three-component LDHs (TC-LDHs) by urea decomposition was carried out under similar experimental conditions previously described for precipitation of α-$Ni(OH)_2$ and Ni/Al LDHs [30,31]. Stock solutions of metal ions (0.8 M in Ni^{2+} and 0.5 M in Co^{2+} and Al^{3+}) were prepared from reagent grade $NiCl_2·6H_2O$, $AlCl_3·6H_2O$ (Fisher Scientific) and $CoCl_2·6H_2O$ (J.T. Baker Chemical Co.). Appropriate volumes of stock solutions were mixed in 1 L Pyrex Brand media bottles and the balance of 500 mL was added up with deionized water (18 MΩ cm). This solution was preheated to 90 ± 1 °C. As a precipitation agent, 90.0900 g of reagent grade urea (Fisher Scientific) was dissolved in 250 mL deionized water and added to the preheated $Ni^{2+}/Co^{2+}/Al^{3+}$ solution. Concentrations of cations were adjusted such that they would add up to 0.1 M in the final

volume (i.e. 750 mL). The solution was digested for 2 h before quenching the reaction in an ice-water bath. Pressure was kept near ambient during digestion, by attaching a balloon to the reaction bottle and the solution was stirred continuously. Precipitates were separated from the mother liquor by centrifugation, washed three times and saved for further analysis after drying at 70 °C. Effects of Co^{2+} and Al^{3+} concentrations were investigated by precipitating LDHs with $Ni_{1-(x+y)}^{2+}/Co_x^{2+}/Al_y^{3+}$, where x and y were varied between 0.00 and 0.25 (refer to Table 1 for sample compositions and identification).

Synthesized powders (≈0.5 g) were aged in 35 mL of 6 M KOH for 1 week in order to monitor the effects of electrolyte solution on stability of structures formed.

2.2. Characterization

Yield of reactions was accessed by measuring percent recovery of metal ions from the solution. Supernatant solutions from the centrifuge were stored at +5 °C for analysis. For [Ni^{2+}] both UV-Vis and ICP spectroscopies were used and results were averaged, whereas [Co^{2+}] and [Al^{3+}] were determined only by ICP.

FTIR data was collected in transmission mode with KBr pellets. Spectra were taken using an air-purged Bomem-Hartmann and Braun-MB 102 unit with 4 cm^{-1} resolution. KBr pellets were prepared by mixing 0.70–0.75 wt.% ground powder into KBr matrix and then pressing to 80 MPa with an evacuable die. Pure KBr was run as the reference. Certain regions in spectra (especially ≈2200 cm^{-1} where C–N of cyanate is located) were analyzed by peak deconvolution details of which are described elsewhere [32].

Structural characterization was made by powder X-ray diffraction (Scintag X1-365) unit with Cu Kα radiation. Crystallite size was determined by X-ray line broadening and using Scherrer expression. Instrumental broadening of the peaks was accounted for by correcting the full width at half maximum (FWHM) values with that of the crystalline silicon reference [33]. Specific surface area of powders was measured with 11-point BET method after outgassing the sample at 100 °C for 12 h (Quantachrome Autosorb-1). Specific surface area values reported are the average of five consecutive runs.

All electrochemical studies were performed using a Radiometer-PGP 201 Potentiostat/Galvanostat unit in combination with a three-electrode cell. Chronopotentiometry experiments were performed in 6 M KOH solutions. A Pt wire electrode was used as the auxiliary electrode while the measurements were referenced to a Hg/HgO electrode. Working electrodes were produced by pressing (85 MPa) an active material paste between two circular porous nickel foams, one of which was initially attached to a Pt wire (current collector). Paste mixture contained active powder along with carbon (60/40 wt.%, respectively) that was kneaded with appropriate amount of PTFE dispersed in

Table 1
TC-LDH compositions studied and the percentage of metal ions recovered from the mother liquors as precipitate[a]

Sample	$[Al^{3+}]_0$	$[Ni^{2+}]_0/[Co^{2+}]_0$	% recovered[b]			Phase[c]	d_{003} (±0.02 Å)		Crystallite size[d] (±0.2 nm)	
			Ni^{2+}	Co^{2+}	Al^{3+}		Fresh	Aged	Fresh	Aged
A1	0.025	0.050/0.025	74	52	89	LDH	7.71	7.70	14.0	14.6
A2		0.060/0.015	75	67	93		7.72	7.70	12.1	12.7
A3		0.070/0.005	87	86	94		7.78	7.71	12.2	13.2
A4		0.075/0.000	78	–	84		7.78	7.75	10.7	11.4
B1	0.015	0.060/0.025	73	52	100	LDH	7.69	7.70	11.2	12.5
B2		0.070/0.015	69	59	100		7.69	7.69	9.9	11.5
B3		0.080/0.005	64	63	100		7.70	7.70	8.8	11.0
B4		0.085/0.000	79	–	100		7.66	7.69	8.0	10.8
C1	0.005	0.070/0.025	65	58	100	α	7.43	7.51	6.9	7.1
C2		0.080/0.015	57	51	100		7.41	7.54	6.5	7.5
C3		0.090/0.005	50	36	100		7.41	7.49	6.4	6.4
C4		0.095/0.000	69	–	100		7.40	NS[e]	6.2	NS
D1	0	0.075/0.025	45	52	–	α	7.23	7.35	7.2	6.7
D2		0.085/0.015	45	59	–		7.21	7.21	6.7	4.8
D3		0.095/0.005	52	66	–		7.19	NS	6.6	NS
D4		0.100/0.000	44	–	–		7.26	NS	6.1	NS

Also given are the calculated interlayer separation and crystallite size along *c*-axis before and after the 1 week aging in 6 M KOH.

[a] Note that D4 and A4 are the compositions that were studied extensively elsewhere [32].

[b] After 2 h of digestion at 90 °C.

[c] Decided by the appearance of the asymmetric peak between 30° and 55° 2θ. An asymmetric peak is due to *turbostratic* α-phase.

[d] Crystallite size along *c*-axis.

[e] Not stable.

water (8.6 wt.%). Carbon provides a conductive path for electron transfer ($Ni(OH)_2$ is a p-type semi-conductor with a limited conductance [34–36]). PTFE acts as a binder for attaching the paste to the foams. The electrodes were encapsulated in a glass rod, which was then sealed from top to prevent the electrolyte wetting the current collector. In the preliminary experiments, electrodes were charged and discharged at $0.2C$ rate up to 150% of the theoretical capacity of β-$Ni(OH)_2$ (289 mAh/g [26,36]) for 12 cycles followed by cycling at six different rates and then finally at C rate for 40 cycles. Once the experimental conditions were set, electrodes were cycled at C rate up to 150% of the theoretical capacity for 40 cycles. Specific capacities are determined by taking the derivative of voltage versus specific current plots and determining the maximum of the derivative. All charge and discharge cycles were performed between 100 and 600 mV against Hg/HgO electrode.

In order to compare the electrochemical performance of TC-LDHs produced in this study to commercial β-$Ni(OH)_2$ a sample from Aldrich was tested under the same conditions. In addition, an interstratified (α–β-phase mixture) $Ni(OH)_2$ sample was produced by titrating a 180 mL aqueous mixture of Ni^{2+} and Co^{2+} (0.09 and 0.01 M in the final solution, respectively) with 40 mL of aqueous mixture of NaOH and Na_2CO_3 (0.14 and 0.06 M in the final solution, respectively) in 60 min at 90 °C. After 60 min of digestion, powders were characterized in the same way as LDH compositions described above.

3. Results

3.1. Recovery

Compositions studied and the percentage of cations that could be recovered from those solutions is summarized in Table 1. Generally, higher fractions of cations were recovered as the concentration of trivalent cation Al^{3+} in the starting solution increases. While all of Al^{3+} was recovered with 0.005 and 0.015 M Al^{3+}, approximately 84–94% of Al^{3+} was incorporated in the precipitate when 0.025 M Al^{3+} was used. However, Ni^{2+} and Co^{2+} recoveries were the highest for these cases. With a composition identical to sample A4 (Table 1) UV-Vis spectroscopic analysis showed that practically all of Ni^{2+} precipitated out in 3 h. Nickel recovery was highest with the highest initial Al^{3+} concentration and in the absence of Co^{2+} (A4 through D4). It seems that a composition with high $[Al^{3+}]_0$ and low $[Co^{2+}]_0$ such as A3, should be a good starting point for electrochemical experiments.

3.2. Structural stability

Typical XRD patterns of β, interstratified α + β, α, and LDHs are given in Fig. 1. It can be seen that layer separation increases, in the same order. Interstratified structure shows that intercalation in a segment of layers decreases the interlayer separation (i.e. basal spacing) in the adjacent layers (to values even smaller than in β due to the 0 0 6 of α-phase). Asymmetric peak due to (1 0) for α peak becomes symmetric
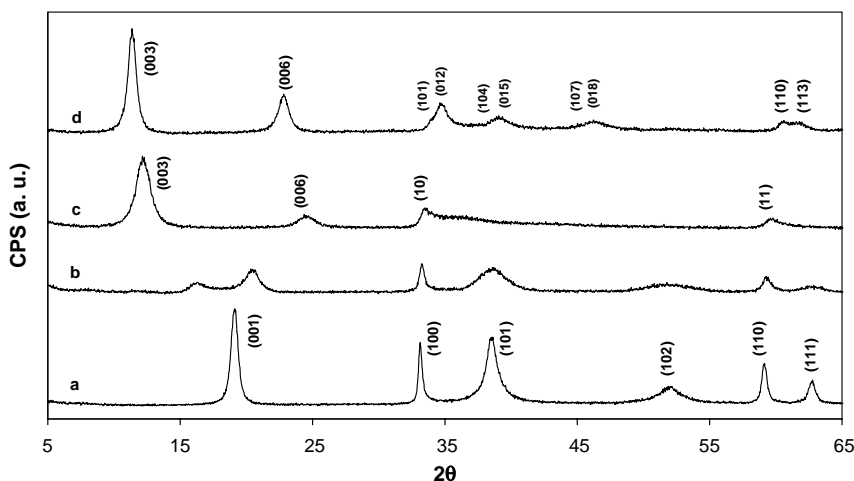
Fig. 1. Typical XRD patterns collected from: (a) β, (b) interstratified α and β, (c) α and (d) LDH phases.

peak (0 1 2) in LDH as layers are aligned in LDH. Results of interlayer separation and crystallite size measurements from all compositions before and after 1 week of aging in 6 M KOH are given in Table 1. An initial Al^{3+} concentration of 0.005 M (C series) was not enough to trigger the formation of LDH phase while 0.015 M was sufficient. While interlayer separation among A and B compositions did not show significant variation, it was notably lower for the C and D series, C being the intermediate. Upon aging, although A series showed a slight decrease in the basal spacing, B series remained unchanged. On the other hand, basal spacing seems to expand in C and D series with aging. Considering that A/B and C/D series give patterns characteristic to α-phase and the LDH, respectively, these differences can be attributed to the different aging mechanisms in these phases. The fact that interlayer separation varies ever so slightly within a series makes reference to the minimal change in the intercalating species coordination chemistry within the series. Except in one composition (A3), crystallite sizes decreased within a series for all series as the $[Co^{2+}]_0$ decreased. Although there was one overlapping result between A and B series, all crystallite sizes measured from A series was larger than B and both were larger than ones measured from C and D series. The differences between C and D series were considerably smaller than the ones among other series.

Ageing consistently increased the crystallite size along the *c*-axis among the LDHs and showed mixed effect on α-phases. With increase in $[Co^{2+}]$, stability of C series (α-phase with insufficient Al^{3+}) improved while the crystallite size either increased or unaltered. On the other hand, in the absence of Al^{3+} transformation to β took place faster and more Co^{2+} was required to slow down the transformation. It is interesting to note that aging decreased the crystallite size of D series (no Al^{3+}). Intuitively, crystal growth with aging was expected. A decrease in crystallite size might imply partial dissolution of α in favor of β-phase. Electrochemical tests were limited to compositions forming stable LDHs.

3.3. Intercalating species

α-$Ni(OH)_2$ and LDHs precipitated by urea decomposition show interesting signatures in the FTIR spectra [32,37]. Features were assigned to hydroxyl stretching in the brucite-type layers (3640 cm^{-1}), hydrogen bonding between intercalating species and the layers, and similar alternatives ending with a hydrogen bond formation (3600–3300 cm^{-1}), C–N stretch of cyanate (2200 cm^{-1}), H–O–H bending mode of water (1600–1650 cm^{-1}), carbonaceous species (1300–1500 cm^{-1}), combination of some modes of carbonaceous species and cyanate deformation mode (620–720 cm^{-1}) and metal–O stretches combined with in-plane OH deformations (400–550 cm^{-1}). From these features, the peak around 2200 cm^{-1} was studied in some detail due to the crucial role of cyanate in the urea precipitated powders. It showed interesting shoulder features that could be attributed to different modes of intercalation of cyanate within the layers. It was demonstrated that relative population of a certain mode could be qualitatively compared to another by looking at the percent area under the relevant mode [32]. Analyses revealed that for LDHs, cyanate remains N-bonded throughout the digestion, while it switches from N-bonded to O-bonded cyanate in the turbostratic α-phase. Similar peak analyses were carried-out for as-prepared powders produced in this study and results are summarized in Table 2. While the population of N-bonded cyanate gradually decreases, that of O-bonded cyanate increases with decreasing $[Al^{3+}]_0$ (i.e. in going from A to D or from LDH to α structure). Trend is most obvious in absorptions assigned to both modes of cyanates at "atop" sites. These results are in excellent agreement with our previous observations. Similar transient features in other absorption peaks were also observed. As an example, the 1300–1500 cm^{-1} region (carbonaceous species and water absorptions) of A4/B4/C4/D4 is depicted in Fig. 2A. It can be seen that carbonate coordination seems to change from free carbonate ion (D_{3h}, a.k.a. tridentate) to uniden-

Table 2
FTIR peak deconvolution results from compositions studied

Adsorption sites[a]	Calculated[a] (cm^{-1})		Series			
			A	B	C	D[b]
O-cyanate, atop	2246	ω_{C-N} (cm^{-1})[c]	2240 ± 2[d]	2256 ± 1	2260 ± 2	2244 ± 3
		% area[e]	10 ± 2[d]	15 ± 4	27 ± 2	39 ± 3
O-cyanate, bridge	2228	ω_{C-N} (cm^{-1})	–	–	–	–
		% area	–	–	–	–
O-cyanate, four-fold	2212	ω_{C-N} (cm^{-1})	2205 ± 1	2214 ± 1	2219 ± 1	2205 ± 0
		% area	26 ± 2	32 ± 3	28 ± 4	11 ± 2
N-isocyanate, atop	2182	ω_{C-N} (cm^{-1})	2182 ± 1	2180 ± 1	2174 ± 2	2176 ± 0
		% area	62 ± 3	50 ± 2	31 ± 2	19 ± 3
N-isocyanate, bridge	2163	ω_{C-N} (cm^{-1})	–	–	–	–
		% area	–	–	–	–
N-isocyanate, four-fold	2151	ω_{C-N} (cm^{-1})	–	–	–	2155 ± 1
		% area	–	–	–	11 ± 2
Other geometries[f]	2057[f]	ω_{C-N} (cm^{-1})	2120 ± 1	2119 ± 1	2115 ± 1	2118 ± 3
		% area	1 ± 0	3 ± 1	10 ± 1	20 ± 2[b]

[a] Calculated positions and assignments are for cyanate adsorbed on Ni(1 0 0) as reported by Yang and Whitten [39]. A detailed discussion can be found elsewhere [32].

[b] Due to the large particle sizes KBr pellets prepared from these samples were not as homogeneous as in others and OCN^- peak was associated with a large background on both sides which could hardly be treated.

[c] Observed position of C–N stretch of cyanate in this work.

[d] Standard deviations were obtained from the four different compositions within one series.

[e] Balance ($\approx 2\%$) is the area under the "artifact" peaks due to CO_2 in the measurement system.

[f] Yang et al. also calculated the energetics of the side-on bonded cyanate and N-bonded cyanate with different tilt angles. It is plausible that this additional mode could be assigned to one of those discussed [39].

tate (C_s) and bidentate (C_{2v}) as the structure changes from LDH to α-phase with decreasing $[Al^{3+}]_0$. Absorptions with all three coordinations seem to appear for the intermediate compositions. It is known that interlamellar carbonate in LDH is surrounded by water molecules. Therefore symmetry of carbonate species in LDH should resemble "free ions" (D_{3h}) [21,38]. It is then expected that a reduction in hydration level should follow a change in carbonate coordi-

nation. On the other hand, an increase in hydration is associated with broadening and elevation of 3300–3600 cm^{-1} band in FTIR spectra (i.e. extensive hydrogen bond formation). Fig. 2B shows the transition in hydration level as the structure changes from LDH to α-phase. Variations in the intercalation chemistry of aged samples and samples submitted to electrochemical tests are subject of future research.
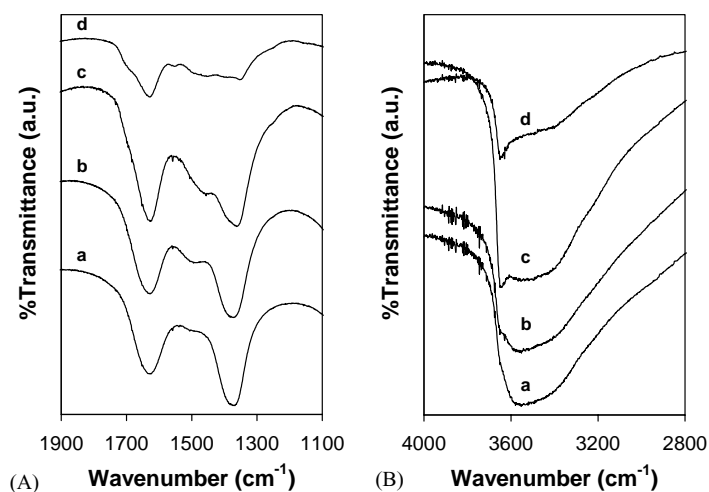

Fig. 2. Evolution of FTIR spectra of (A) carbonaceous species and (B) water around the 3300–3600 cm^{-1} region (indicating hydration level) observed in samples: (a) A4, (b) B4, (c) C4 and (d) D4.

Table 3
Specific surface areas of select samples

Sample	Surface area[a]	s[b]
β-Ni(OH)$_2$	14.6	0.3
Interstratified (α + β)	111.5[c]	–
A1	55.7	0.9
A2	58.8	0.5
A3	55.7	0.6
A4	65.7	0.7
B3	85.0	3.4
D4	94.6	1.7

[a] Specific surface area measured by 11-point BET method in m^2/g.
[b] Sample standard deviation from five consecutive runs.
[c] Average of two runs.

3.4. Specific surface area

Results of specific surface area measurements from select samples are given in Table 3. For the A series, there is no identifiable trend, however both B3 and D4 were slightly higher than all A compositions. While all compositions tested had notably higher surface areas with respect to β-phase, sample with the interstratified structure showed an even higher surface area compared to these compositions. Although surface area itself is not indicative of powder's capacity as electrode material, for a given composition and structure, higher the surface area higher the rate, and higher capacity.

3.5. Capacity measurements

Judging by the percentage of metal ions recovered from the solution, sample A3 seemed to provide the optimum synthesis conditions. Therefore, electrochemical tests were carried out with this sample. First, the effect of Al^{3+} was studied by comparing A3 ([A^{3+}]$_0$ = 0.025 M) with B3 ([A^{3+}]$_0$ = 0.015 M), both of which had same [Co^{2+}]$_0$ = 0.005 M. Results of initial 12 cycles with 0.2C rate are summarized in Figs. 3 and 4. Also depicted is the performance
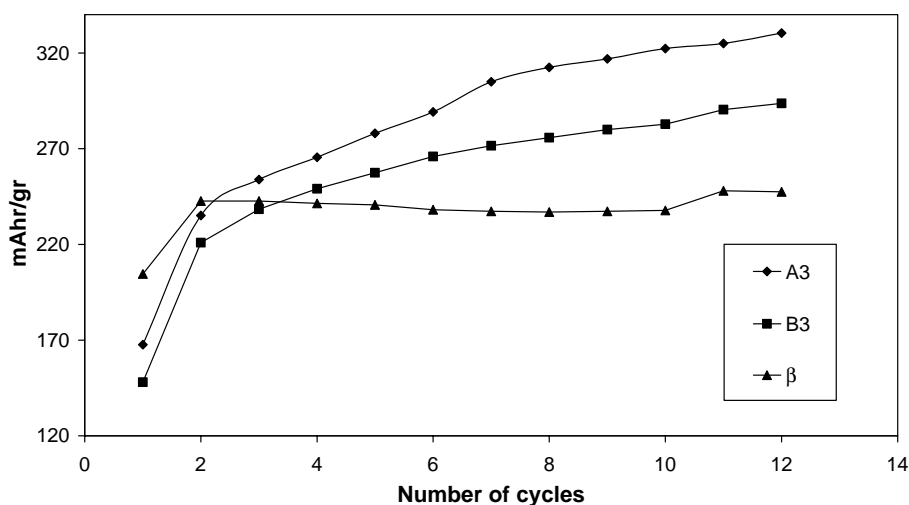

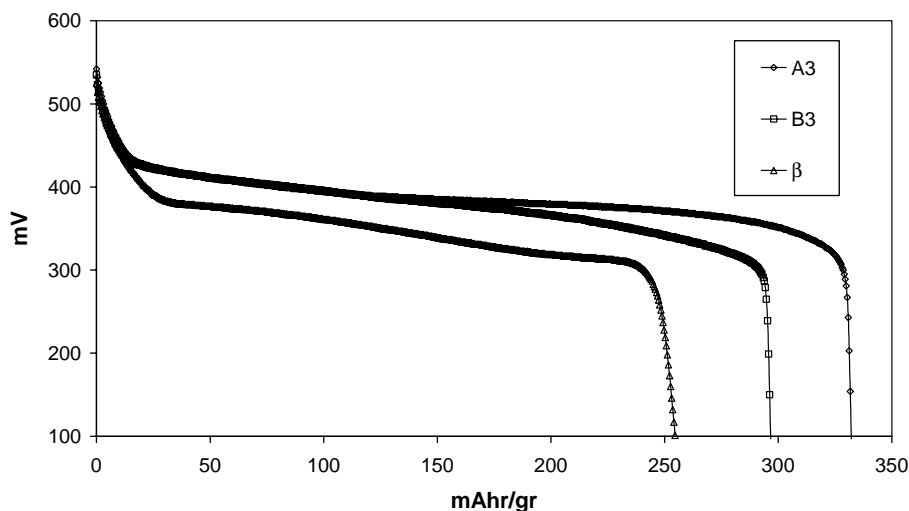Fig. 3. Capacities measured from initial 12 cycles (at 0.2C rate) for samples A3, B3 and β-phase.

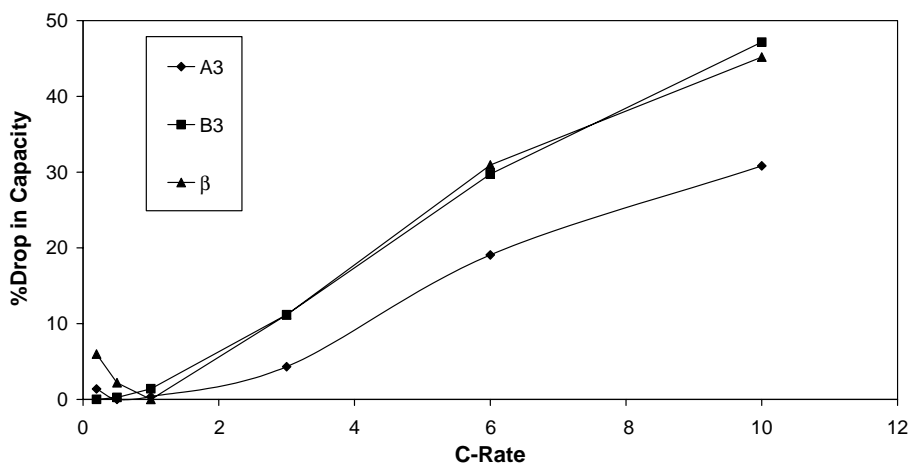Fig. 4. Twelfth cycles from Fig. 3 at 0.2C rate from samples A3, B3 and β-phase.

Fig. 5. Percent drop in capacity of samples A3, B3 and β-phase with increasing discharge rates.

of β-phase (Aldrich Chemical Company) under identical conditions. Measured values are subject to 5% error due variations in electrode preparation. Although β-phase reached its stabilized capacity faster than the LDHs, the latter outperformed the β-phase after a relatively short number of cycles. It is also important that both LDHs delivered their high capacities at higher and more stable voltages. β-Phase investigated in this work had displayed signatures from intercalated water and carbonate in its FTIR spectra. Although it was determined to be X-ray phase-pure it is not clear if there is a slight interstratification with α-phase or surface adsorption. It was recently noted that interstratified structures could deliver higher specific capacities [4]. Observation of surprisingly high specific capacity from β-phase (≈90% of theoretical capacity) invokes the possibility of a slight interstratification and/or optimized electrode preparation method.

Percent drop in capacity with increasing discharge rates is a parameter that has significance in practical applications. Fig. 5 shows the drop in capacity of the same samples at six different rates. At around C rate the drop was not significant for any of the samples. In addition, the drops observed at relatively higher rates were comparable to what is reported in literature [28]. It is also noted that at higher discharge rates the capacity drop in A3 was smaller compared to that in B3 and the β-phase.

Long-term electrochemical stability is one of the most important characteristics of electrode material. Fig. 6 presents the charge capacity of the three samples for 40 cycles at C rate. All compositions delivered relatively stable capacities. In addition, A3 continued to exhibit the highest capacity of the three.

As A3 showed the highest capacity and electrochemical stability, the effect of Co^{2+} content was determined by subjecting the A1/A2/A4 to 40 cycles at C rate. Results are compared to that from the similarly treated interstratified (α + β) sample in Fig. 7. The results indicate that the initial 12 cycles and the cycles at different rates applied to A3, B3 and β-phase prior to the subsequent 40 cycles bring these
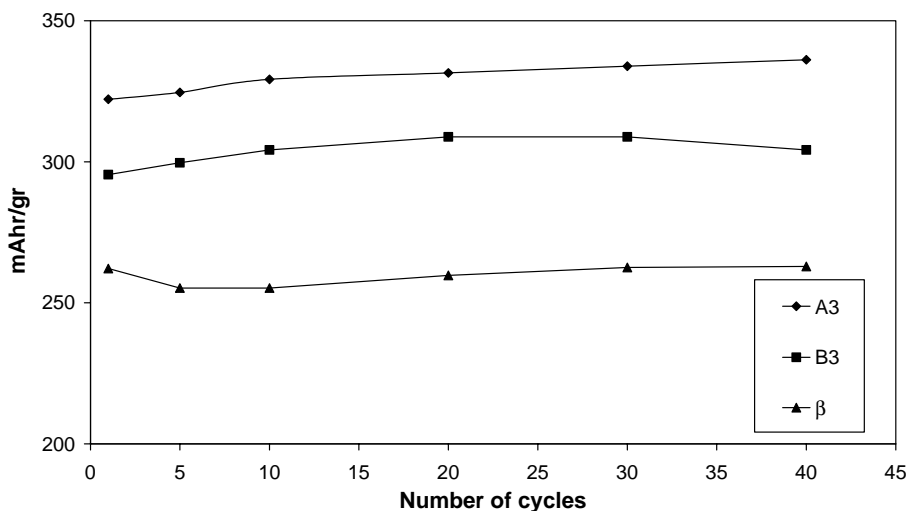

Fig. 6. Effect of 40 additional cycles at C rate on capacities of samples A3, B3 and β-phase.
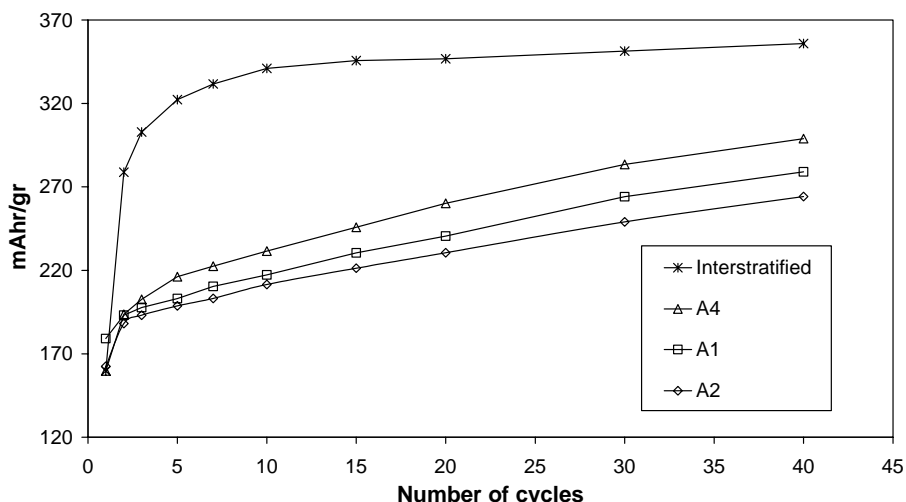
Fig. 7. Changes in capacities of samples in series A (A1, A2 and A4) compared with changes in interstratified ($\alpha + \beta$) phase (40 cycles at *C* rate).

samples to the stable capacities. However starting with 40 cycles at *C* rate was not sufficient to achieve the stable capacities for the samples shown in Fig. 7. The increasing trend in capacities was notable, however the difference among A1, A2 and A3 was subtle. Considering the effects of processing parameters on the particle morphology and intercalate chemistry [32], these differences were believed to be within the experimental error. In contrast to A series, the interstratified ($\alpha + \beta$) sample reached its stable capacity within the first 40 cycles and exhibited the highest specific capacity attained in this study. Highest capacities reached by all samples are summarized in Table 4. Note that although the results from the two sets of schedules cannot be compared directly, it is possible to evaluate interstratified sample and the samples in the first set together. It is also obvious that all compositions performed better than the β-phase. While the capacity measured from A2 was only 1 mAh/g higher than that from β, we can assume that A2 would deliver higher capacities upon further cycling.

Table 4
Maximum specific capacity measured for compositions tested with two different cycling schedules

Sample	Specific capacity[a]
A3[b]	336
B3[b]	304
β-Ni(OH)$_2$[b]	263
Interstratified ($\alpha + \beta$)[b]	356
A4[c]	299
A1[c]	279
A2[c]	264

[a] In units of mAh/g.
[b] Stabilized values.
[c] Stabilized value was not achieved.

Fig. 8 depicts the 40th discharge cycle from sample with interstratified structure and samples A1, A2 and A4. It is evident that Ni/Al LDH delivers its capacity at a higher voltage than the others. Three-component LDHs discharge at intermediate voltages while the interstratified structure
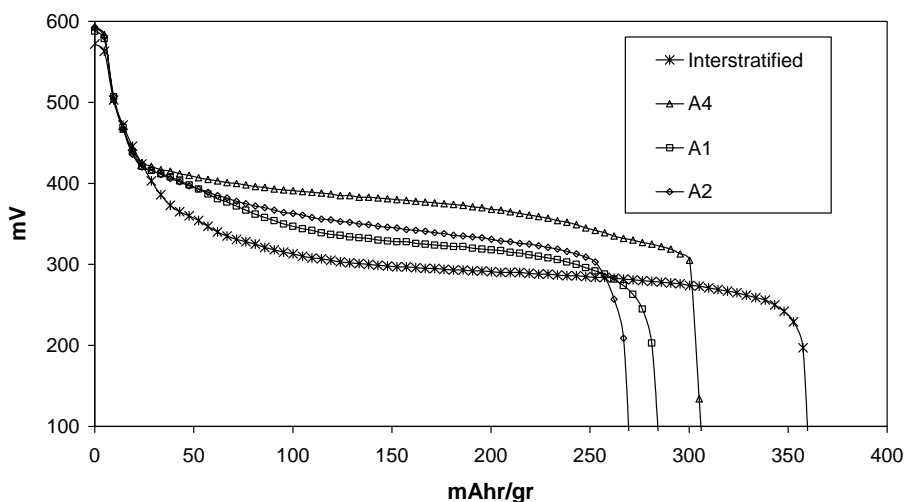

Fig. 8. Fortieth discharge cycle from samples A1, A2 and A4 is compared with that of interstratified phase (40 cycles at *C* rate).

supply its capacity at a considerably lower voltage compared to all samples in this group.

4. Discussion

It was shown experimentally that Ni–Al LDHs could be precipitated by urea decomposition in aqueous solutions [22,32]. XRD and FTIR results suggest that urea could also be utilized in precipitating three-component LDHs incorporating Co^{2+} in addition to Ni–Al.

A 2-h digestion was sufficient to precipitate 0.015 M aluminum completely but not 0.025 M. This suggests that at an intermediate $[Al^{3+}]_0$ (i.e. ≈ 0.020 M), all of aluminum along with maximum amount of Ni^{2+} and Co^{2+} will be recovered. Similarly, Ni^{2+} could be precipitated completely in about 3 h under experimental conditions similar to A4. In addition, incorporation of up to 40% Al^{3+} into the basal planes have been reported [40]. It can be proposed that use of even higher $[Al^{3+}]_0$ would result in complete recovery of other cations in less than 3 h. Nevertheless, as the M^{3+} incorporation increases the amount of M^{2+} that would be available for electrochemical cycling would decrease per mass of material. Intuitively, keeping the M^{3+} at a minimum while preserving the structural integrity would be desirable in the delivery of highest possible capacity.

For the formation of LDHs an initial Al^{3+} concentration of 0.015 M was needed. Presence of Co^{2+} did not impede the formation of LDHs. Basal plane spacing remained similar in LDHs upon aging, but it was expanded in α-phase. Crystallite sizes decreased or remained unaffected in α-phase with aging, but there was a notable increase in LDHs. This suggests that once the LDH forms, it is a highly stable structure in the electrolyte. With higher $[Al^{3+}]_0$ larger crystallites were obtained. This hints a strain-free stacking of layers. With a couple of exceptions, Co^{2+} seems to trigger a faster crystallite growth in the *c*-axis. Results presented in this work are insufficient to suggest a self-consistent mechanism.

FTIR results provide evidence for co-intercalation of water, cyanate and carbonaceous species. Most of cyanate seems to be bonded through its nitrogen in LDHs while it stays mostly oxygen bonded in α-phase and mixed-mode for the compositions in between. Yang and Whitten found that N-isocyanate was energetically more stable at all sites on Ni(1 0 0) compared to O-isocyanate. This is in line with the observed stability of LDHs in the electrolyte [39].

It is proposed that water molecules can be removed reversibly without destroying the LDH structure [41]. Given the hydration level differences observed in A3 and B3 (similar to A4 and B4 that were depicted in Fig. 2B), it is plausible to attribute the capacity difference observed between these samples to the availability of water that could be reversibly exchanged during cycling.

In general all LDH compositions exhibited better electrochemical characteristics than the β-phase. On the other hand, it was noted that they reached their stable capacities more

slowly. It was shown by mathematical models on $Ni(OH)_2$ electrodes that response of the electrode in cyclic voltammetry is more sensitive compared to its response in chronopotentiometry to changes in the diffusion constant of the active species [42]. For that reason, attributing the higher capacities observed in LDHs to the higher diffusivities of the active species cannot be claimed without cyclic voltammetry data. Reproducible results obtained in cyclic chronopotentiometry may be attributable to long-term stability of LDHs in the aggressive electrolyte. It is believed that the procedural differences among different research groups make a quantitative comparison of results doubtful if not impossible.

We have not recorded a substantial improvement by the addition of Co^{2+} in the Ni–Al LDH. It could be thought that once the stability is attained and electrode construction is optimized (with carbon addition) under near-equilibrium testing conditions, there is no added advantage of increasing basal plane conductivity. Absence of pronounced effect of Co^{2+} on capacity may be attributable to either the fact that process is not controlled via electron transport and the electrode construction provides an unobstructed pathway for electron flow (i.e. Co^{2+} is not needed), or benefit provided by Co^{2+} is compromised by the decreased amount of active Ni^{2+} ions that are available for cycling (i.e. Co^{2+} irreversibly oxidizes to Co^{3+} and does not participate in the redox process).

Sample with the interstratified structure showed an exceptionally high capacity compared to all other samples. Besides, although it delivered this capacity at a lower voltage it was the fastest to stabilize. These observations are in agreement with what Wang et al. has recently reported [4]. It is not known with what mechanism capacities of this magnitude can be achieved in such structures. It is entirely possible that the high specific surface area obtained for this sample may have contributed to the observed superior capacity. This hypothesis needs to be checked rigorously.

5. Conclusions

Precipitation of TC-LDH with Ni/Al/Co is proven conceptually by the urea precipitation method. A minimum initial Al^{3+} concentration of 0.015 M is necessary for the formation of LDH structure when total metal ion concentration is set to 0.1 M. All compositions leading to LDH formation proved to be stable in the electrolyte solution for at least 1 week and showed no signs of transformation to β-phase. Previous findings on the role of OCN^- coordination in precipitation of $Ni(OH)_2$ by urea were supported with the detailed FTIR studies performed on TC-LDH studied here. N-bonded cyanates were found to dominate any other cyanate species in the LDHs. Addition of Co^{2+} does not impede the LDH formation and stability of the structure. On the other hand, added basal plane conductivity with the incorporation of Co^{2+} does not seem to enhance the capacity of the powders. While capacities

obtained from all LDH compositions were higher than that from β-phase, interstratified phase produced by heterogeneous precipitation showed the highest capacity attained in this study. Additional work is necessary to understand the mechanism leading to the observation of capacities of this magnitude.

Acknowledgements

References

[1] M. Rajamathi, P.V. Kamath, R. Seshadri, J. Mater. Chem. 10 (2000) 503.
[2] G.J.d.A.A. Soler-Illia, M. Jobbagy, A.E. Regazzoni, M.A. Blesa, Chem. Mater. 11 (1999) 3140.
[3] Q. Song, Z. Tang, H. Guo, S.L.I. Chan, J. Power Sources 112 (2002) 428.
[4] X. Wang, H. Luo, P.V. Parkhutik, A.-C. Millan, E. Matveeva, J. Power Sources 115 (2003) 153.
[5] R.S. Jayashree, P.V. Kamath, J. Power Sources 107 (2002) 120.
[6] M. Rajamathi, P.V. Kamath, Int. J. Inorg. Mater. 3 (2001) 901.
[7] J. Wang, A.G. Kalinichev, R.J. Kirkpatrick, X. Hou, Chem. Mater. 13 (2001) 145.
[8] V.R.L. Constantino, T.J. Pinnavaia, Inorg. Chem. 1995 (1995) 34.
[9] X. Hou, R.J. Kirkpatrick, Chem. Mater. 12 (2000) 1890.
[10] C. Faure, C. Delmas, P. Willmann, J. Power Sources 35 (1991) 263.
[11] C. Faure, C. Delmas, M. Fouassier, P. Willmann, J. Power Sources 35 (1991) 249.
[12] B.S. Maruthiprasad, M.N. Sastri, S. Rajagopal, K. Seshan, K.R. Krishnamurthy, T.S.R.P. Rao, Proc. Indian Acad. Sci., Chem. Sci. 100 (1988) 459.
[13] M.J. Avena, M.V. Vazquez, R.E. Carbonio, C.P. De Pauli, V.A. Macagno, J. Appl. Electrochem. 24 (1994) 256.
[14] M. Dixit, G.N. Subbanna, P.V. Kamath, J. Mater. Chem. 6 (1996) 1429.
[15] A. Widjaja, Synthesis and characterization of nickel hydroxide powders for battery applications, M.Sc. Thesis, Iowa State University, Ames, 1997.
[16] M. Akinc, N. Jongen, J. Lemaitre, H. Hofmann, J. Eur. Ceram. Soc. 18 (1998) 1559.
[17] R. Acharya, T. Subbaiah, S. Anand, R.P. Das, Mater. Lett. 57 (2003) 3089.
[18] R. Acharya, T. Subbaiah, S. Anand, R.P. Das, Mater. Chem. Phys. 81 (2003) 45.
[19] I. Yazdi, Synthesis and electrochemical studies of cobalt substituted nickel hydroxide for battery applications, M.Sc. Thesis, Iowa State University, Ames, 1999.
[20] P.V. Kamath, M. Dixit, L. Indira, A.K. Shukla, V.G. Kumar, N. Munichandraiah, J. Electrochem. Soc. 141 (1994) 2956.
[21] K.T. Ehlsissen, A. Delahaye-Vidal, P. Genin, M. Figlarz, P. Willmann, J. Mater. Chem. 3 (1993) 883.
[22] U. Costantino, F. Marmottini, M. Nocchetti, R. Vivani, Eur. J. Inorg. Chem. 1998 (1998) 1439.
[23] B. Liu, X.Y. Wang, H.T. Yuan, Y.S. Zhang, D.Y. Song, Z.X. Zhou, J. Appl. Electrochem. 29 (1999) 855.
[24] R. Roto, G. Villemure, J. Electroanal. Chem. 527 (2002) 123.
[25] C.Y. Wang, S. Zhong, K. Konstantinov, G. Walter, H.K. Liu, Solid State Ionics 148 (2002) 503.
[26] Z. Hengbin, L. Hansan, C. Xuejing, L. Shujia, S. Chiachung, Mater. Chem. Phys. 79 (2003) 37.
[27] T. Pan, J.M. Wang, Y.L. Zhao, H. Chen, H.M. Xiao, J.Q. Zhang, Mater. Chem. Phys. 78 (2003) 711.
[28] H. Chen, J.M. Wang, T. Pan, H.M. Xiao, J.Q. Zhang, C.N. Cao, Int. J. Hydrogen Energy 27 (2002) 489.
[29] C.Y. Wang, S. Zhong, D.H. Bradhurst, H.K. Liu, S.X. Dou, J. Alloys Compd. 330–332 (2002) 802.
[30] B. Mavis, M. Akinc, Key Eng. Mater., in press.
[31] B. Mavis, M. Akinc, Ceram. Eng. Sci. Proc. 24 (2003) 117.
[32] B. Mavis, M. Akinc, Mater. Chem. Phys., submitted for publication.
[33] F. Boulc'h, M.-C. Schouler, P. Donnadieu, J.-M. Chaix, E. Djurado, Image Anal. Stereol. 20 (2001) 157.
[34] P.M. Gomadam, J.W. Weidner, R.A. Dougal, R.E. White, J. Power Sources 110 (2002) 267.
[35] V. Srinivasan, J.W. Weidner, R.E. White, J. Solid State Electrochem. 4 (2000) 367.
[36] A.B. Yuan, N.X. Xu, J. Appl. Electrochem. 31 (2001) 245.
[37] B. Mavis, M. Akinc, J. Am. Ceram. Soc., submitted for publication.
[38] A.S. Prakash, P.V. Kamath, M.S. Hegde, Mater. Res. Bull. 35 (2000) 2189.
[39] H. Yang, J.L. Whitten, Surf. Sci. 401 (1998) 312.
[40] D.R. Hines, G.T. Seidler, M.M.J. Treacy, S.A. Solin, Solid State Commun. 101 (1997) 835.
[41] V.R. Allmann, Chimia 24 (1970) 99.
[42] K.P. Ta, J. Newman, J. Electrochem. Soc. 145 (1998) 3860.